Electronic Supplementary Material (ESI) for New Journal of Chemistry.

Supporting Information For:

Rapid Recognition of Fatal Cyanide in Water in a Wide pH Range by a Trifluoroacetamido Based Metal-Organic Framework

Abhijeet Rana,[a] Chiranjib Gogoi,[a] Subhrajyoti Ghosh,[a] Soutick Nandi,[ab] Saurav Kumar,[a] Uttam Manna and Shyam Biswas[a]*

[a]Department of Chemistry, Indian Institute of Technology Guwahati, Guwahati, 781039 Assam, India.

[b]Department of Chemistry, Brainware University, Kolkata, 700125 West Bengal, India.

* Corresponding author. Tel: +91-3612583309, Fax: +91-3612582349.

E-mail address: sbiswas@iitg.ac.in

Materials and General Methods:

All the reagents and solvents were purchased from commercial available sources and used without further purification, except the $H_2BDC\text{-}NHCOCF_3$ ligand which was prepared according to the reported procedure.[1] The initial reagents for the synthesis of $H_2BDC\text{-}NHCOCF_3$ ligand, namely 4-aminobenzoic acid and trifluoroacetic anhydride, were purchased from Sigma Aldrich Chemical Co. and Loba Chemie Pvt. Ltd, respectively. Fourier transform infrared (FT-IR) spectra were collected in the region 400-4000 cm^{-1} on a PerkinElmer Spectrum Two FT-IR spectrometer. The following notations were used for characterization of the bands: broad (br), strong (s), very strong (vs), medium (m) and weak (w). FE-SEM images were captured with a Zeiss (Zemini) scanning electron microscope. Thermogravimetric analyses (TGA) were performed under air atmosphere at a heating rate of 5 °C min^{-1} in a temperature region of 25-700 °C by employing a Netzsch STA-409CD thermal analyser. Rigaku Smartlab X-ray diffractometer (model TTRAX III) was employed for powder X-ray diffraction (XRD) measurements at 50 kV, 100 mA using Cu-*K*α (λ = 1.5406 Å) radiation. N_2 sorption isotherms were recorded by using Quantachrome Quadrasorb evo surface area analyser at −196 °C. Before the sorption analysis, the degassing of the compound was carried out at 100°C under high vacuum for 12 h. The contact angle measurements were performed by employing a KRUSS Drop Shape Analyzer-DSA-25 instrument with an automatic liquid dispenser at ambient temperature. Fluorescence sensing studies were performed with a HORIBA JOBIN YVON Fluoromax-4 spectrofluorometric). The DIVCOL program[2] incorporated within STOE's WinXPow software package[3] was used to determine the lattice parameters. Pawley refinement was carried out using Materials Studio software.

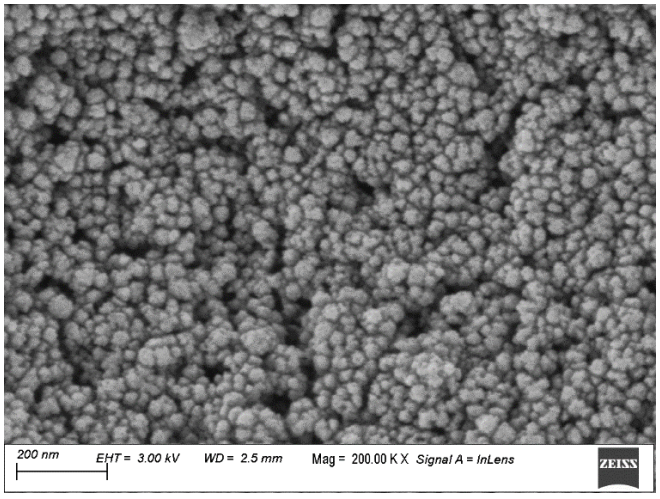

Figure S1. FESEM image of **1′**.

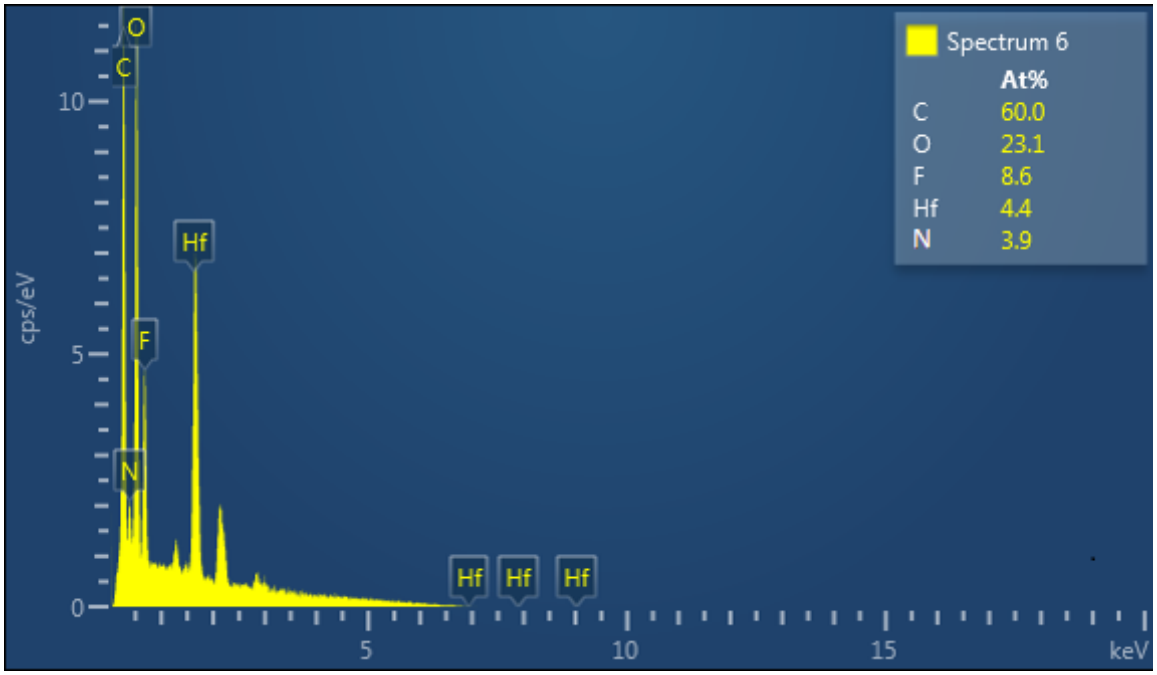

Figure S2. EDX spectrum of **1′**.

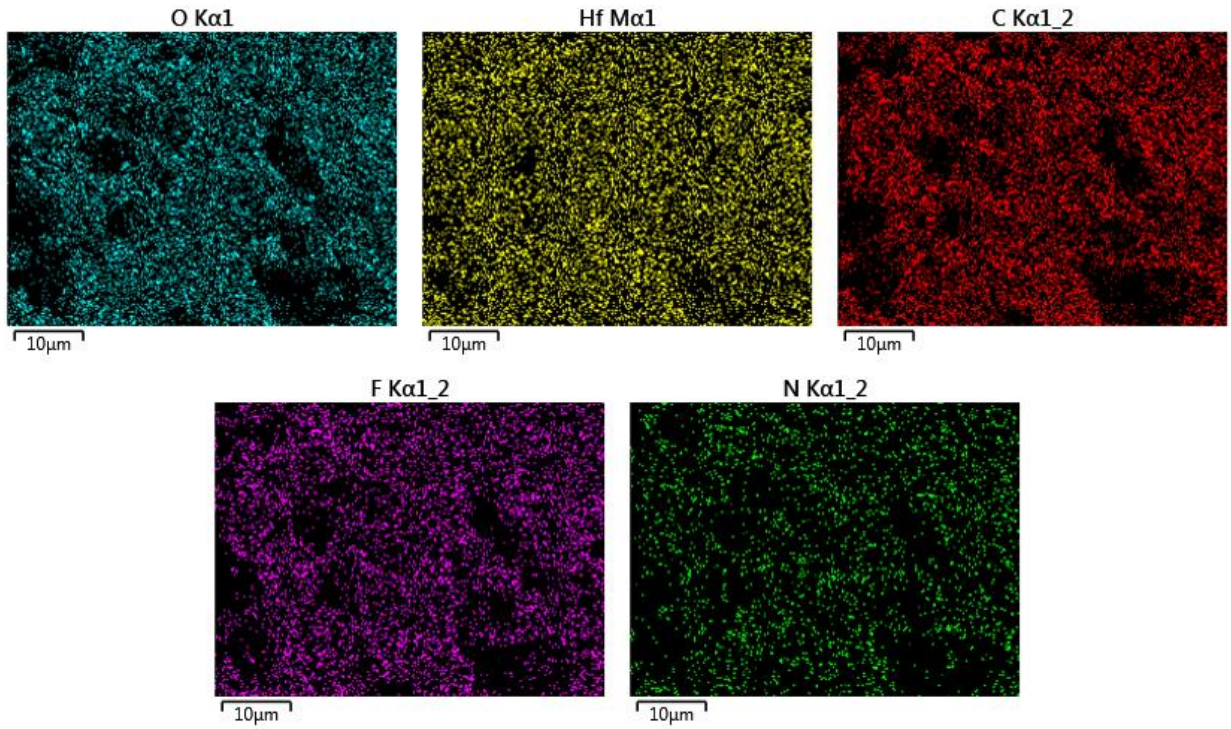

Figure S3. EDX elemental mapping of **1′**.

Table S1. Unit cell parameters of **1** obtained by indexing its PXRD data collected at room temperature. The obtained values have been compared with the PXRD data of UiO-66 MOF collected at room temperature.

Compound name	$[Hf_6O_4(OH)_4(BDC\text{-}NH\text{-}COCF_3)_6]\cdot 4H_2O\cdot 5DMF$ (**1**) (this work)	UiO-66 (reported)[4]
Space Group	$Fm\bar{3}m$ (225)	$Fm\bar{3}m$ (225)
Crystal System	Cubic	Cubic
a = b = c (Å)	20.748 (3)	20.700 (2)
α = β= γ (°)	90	90
V ($Å^3$)	8931.0 (19)	8870.3 (2)
Radiation	Cu Kα1	Cu Kα1
Figure of Merit (FOM)	39.4	-

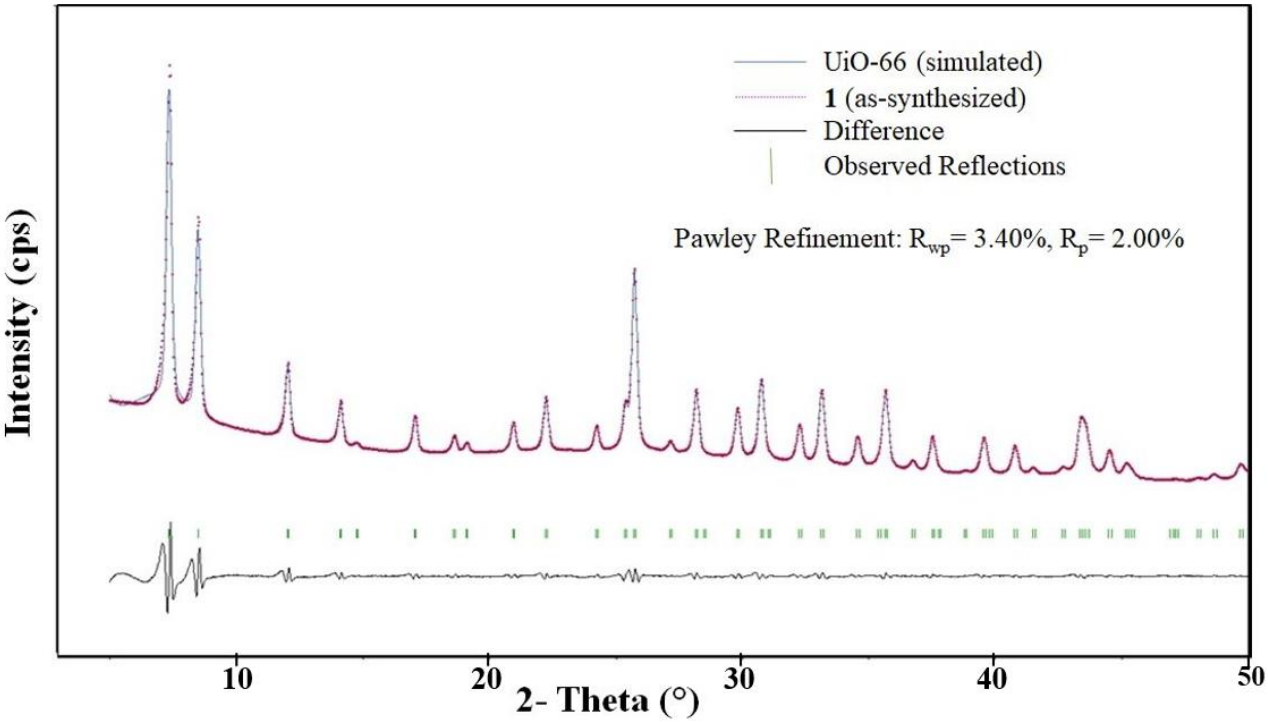

Figure S4. Pawley fit for the XRPD pattern of as-synthesized **1**. Blue lines and red dots denote simulated and observed patterns, respectively. The peak positions and difference plot are displayed at middle (R_p = 2.00, R_{wp} = 3.40).

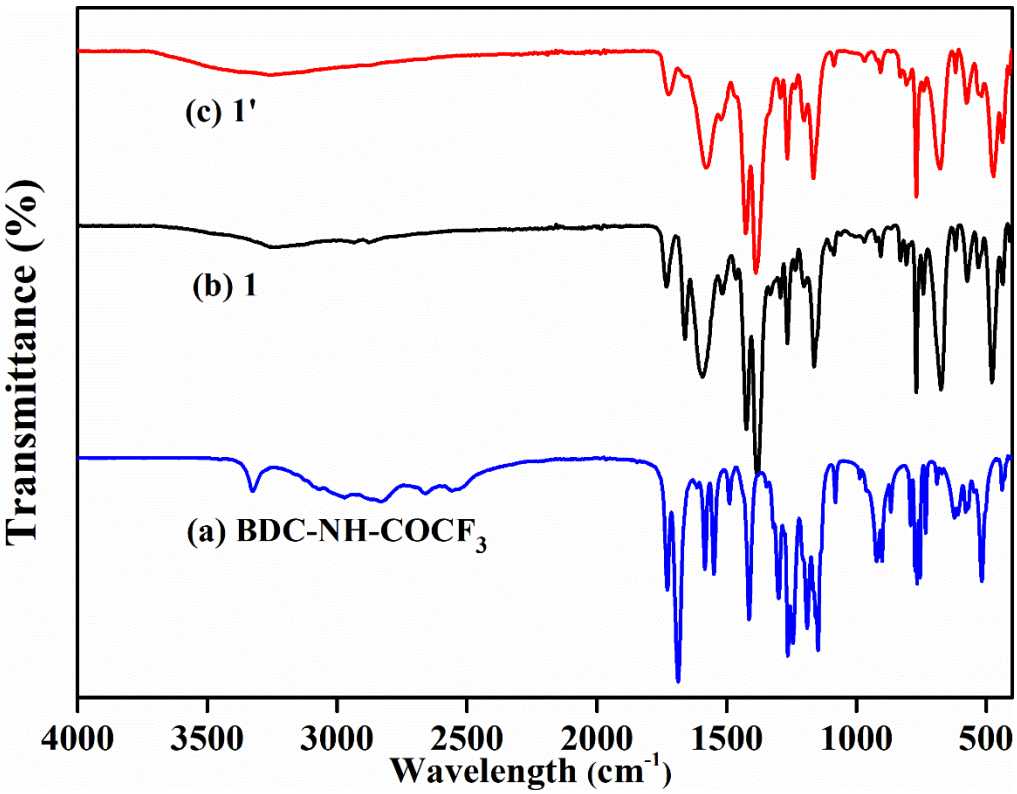

Figure S5. FT-IR spectra of (a) H_2BDC-NH-$COCF_3$ ligand (blue), (b) as-synthesized **1** (black) and (c) activated **1′** (red).

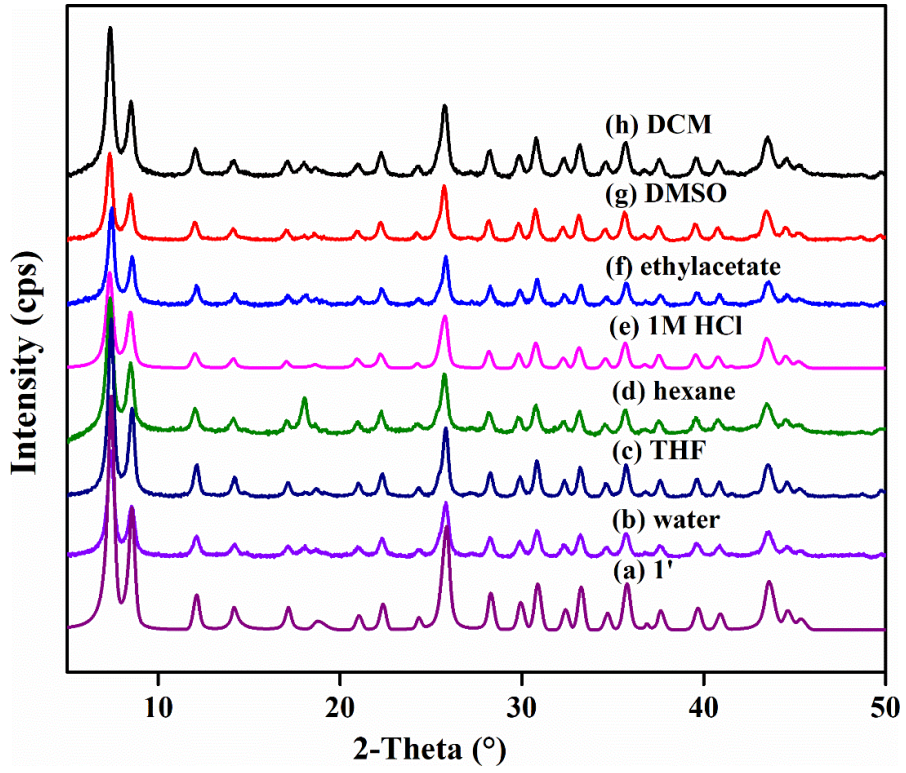

Figure S6. PXRD patterns of **1′** showing its chemical stability in (b) water, (c) THF, (d) hexane, (e) HCl (1M), (f) ethyl acetate, (g) DMSO and (h) DCM.

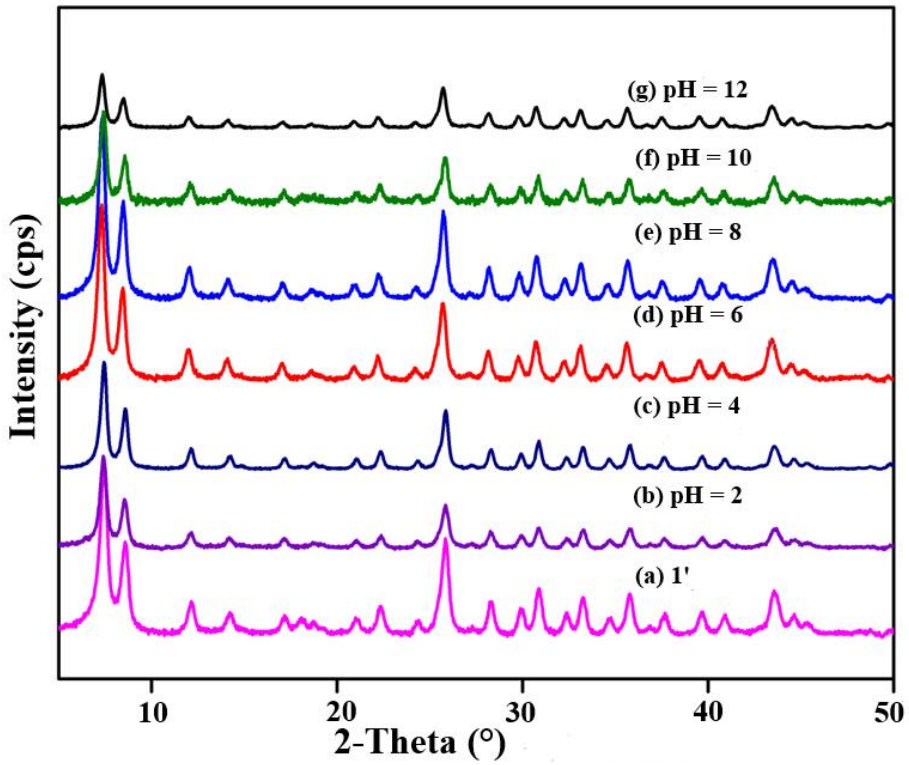

Figure S7. PXRD patterns of **1′** showing its chemical stability in different pH media.

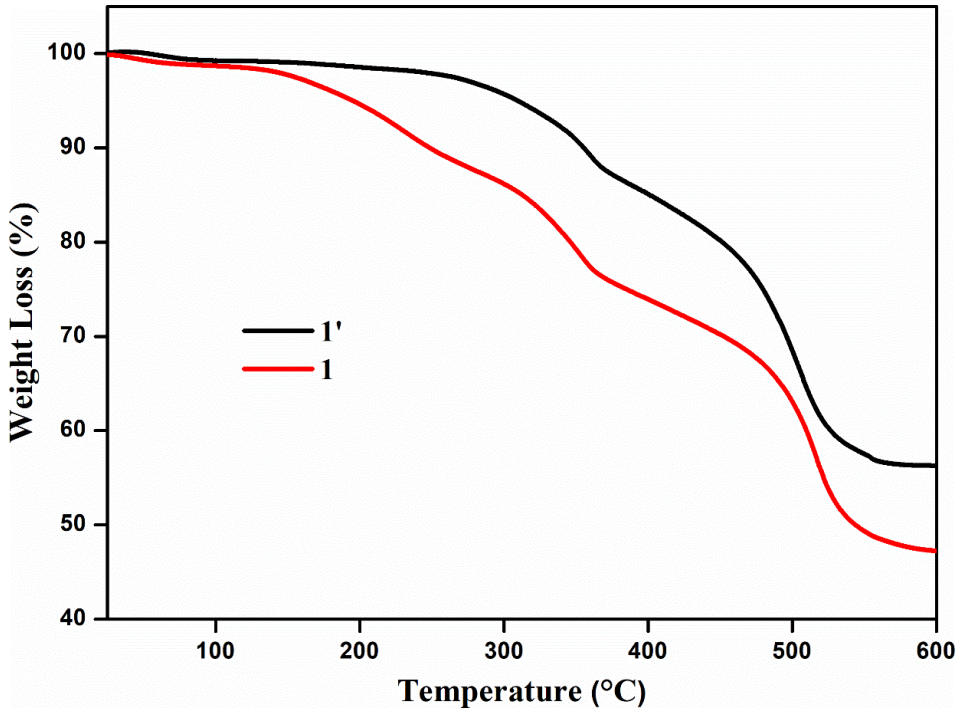

Figure S8. TGA curves of as-synthesized **1** (red) and activated **1′** (black) recorded in an air atmosphere in the temperature range of 25-600 °C at a heating rate of 5 °C min^{-1}.

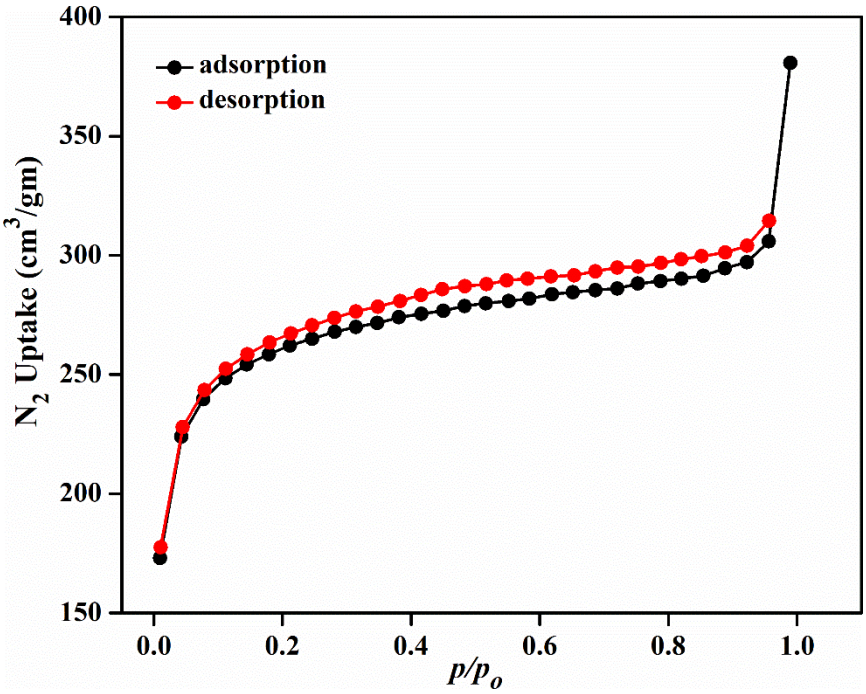

Figure S9. N_2 adsorption (black circles) and desorption (red circles) isotherms of thermally activated **1′** recorded at –196 °C.

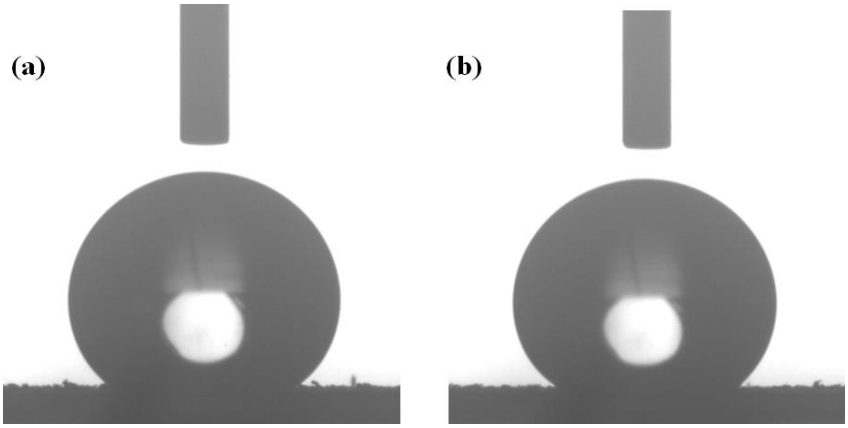

Figure S10. The contact angle images of beaded water droplets on the surface of (a) **1** and (b) **1′**.

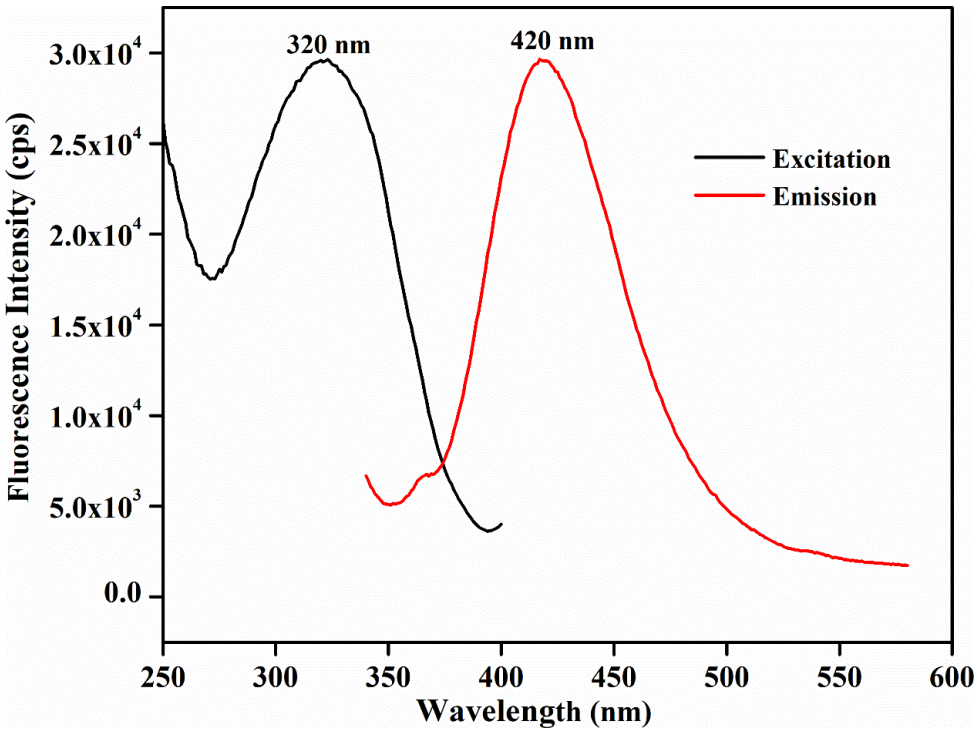

Figure S11. Fluorescence excitation (black) and emission (red) spectra of **1′**.

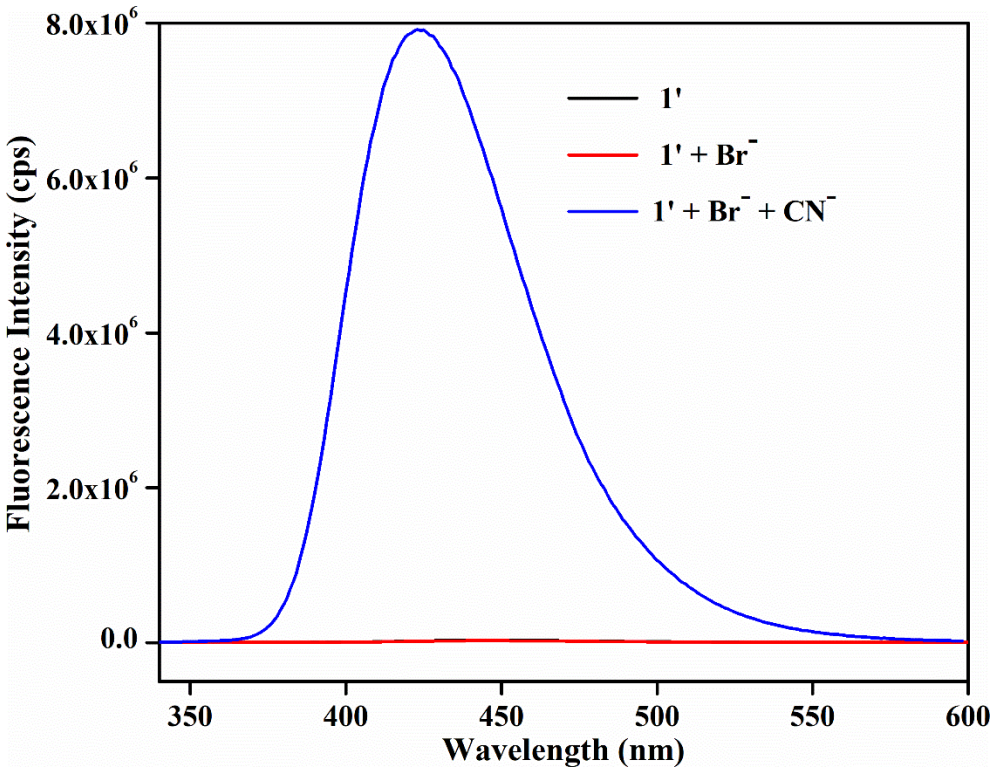

Figure S12. Fluorescence intensity of **1′** dispersed in water after addition of 10 mM solution of NaCN in water (300 µL) in presence of 10 mM solution of NaBr in water (300 µL).

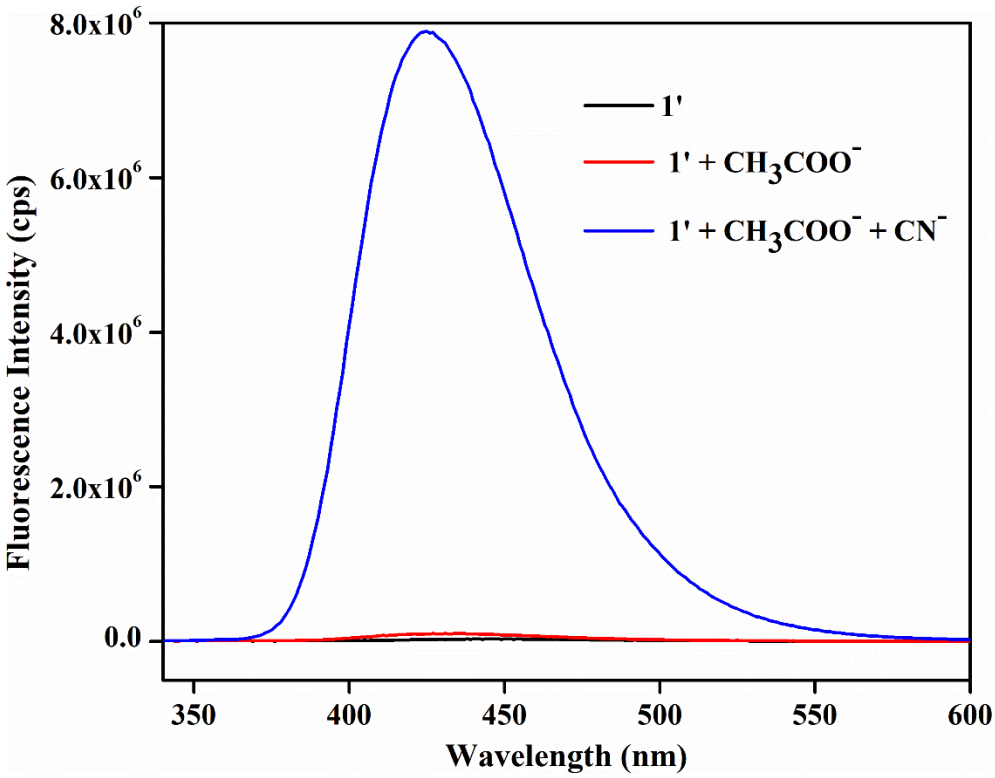

Figure S13. Fluorescence intensity of **1′** dispersed in water after addition of 10 mM solution of NaCN in water (300 µL) in presence of 10 mM solution of CH_3COONa in water (300 µL).

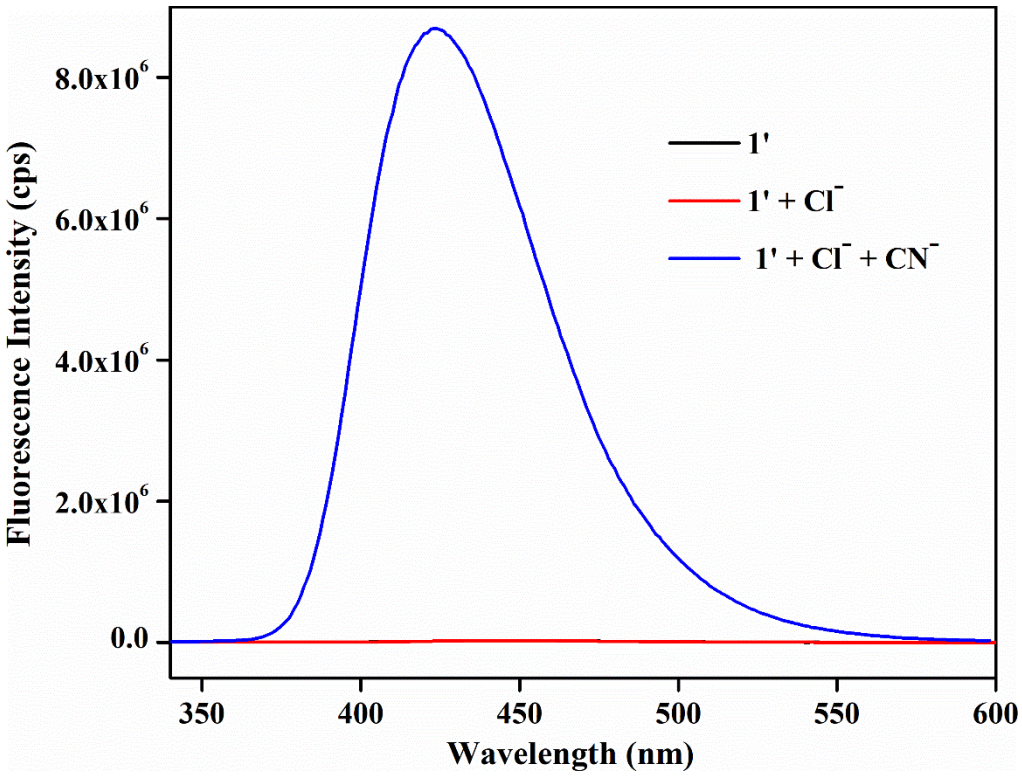

Figure S14. Fluorescence intensity of **1′** dispersed in water after addition of 10 mM solution of NaCN in water (300 µL) in presence of 10 mM solution of NaCl in water (300 µL).

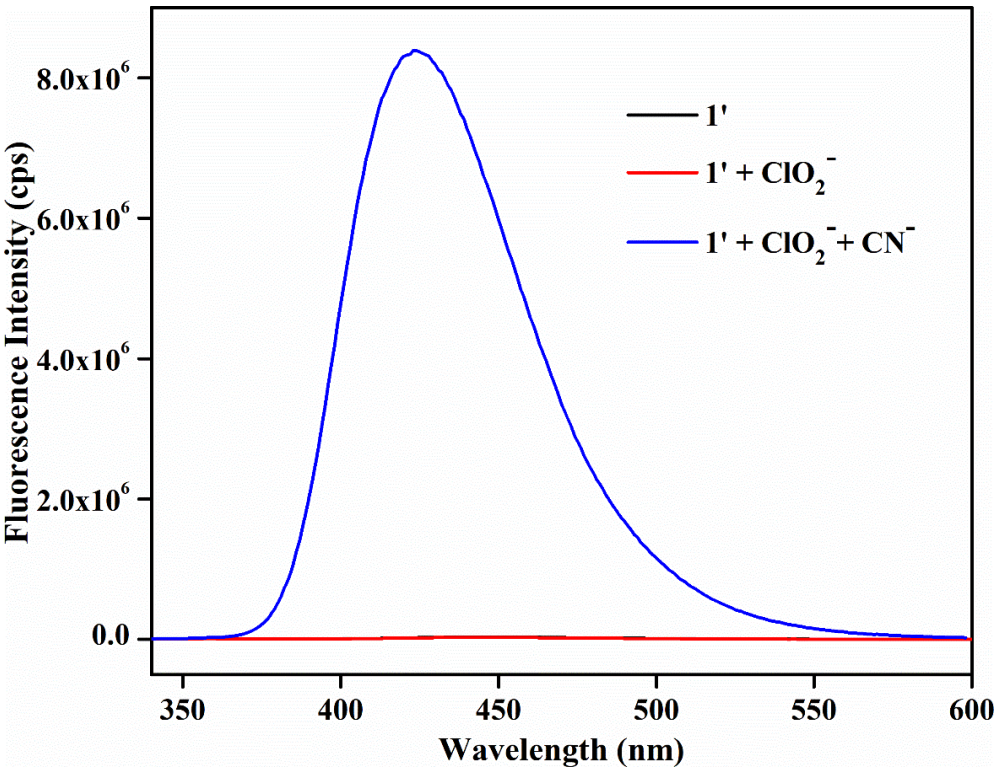

Figure S15. Fluorescence intensity of **1′** dispersed in water after addition of 10 mM solution of NaCN in water (300 µL) in presence of 10 mM solution of $NaClO_2$ in water (300 µL).

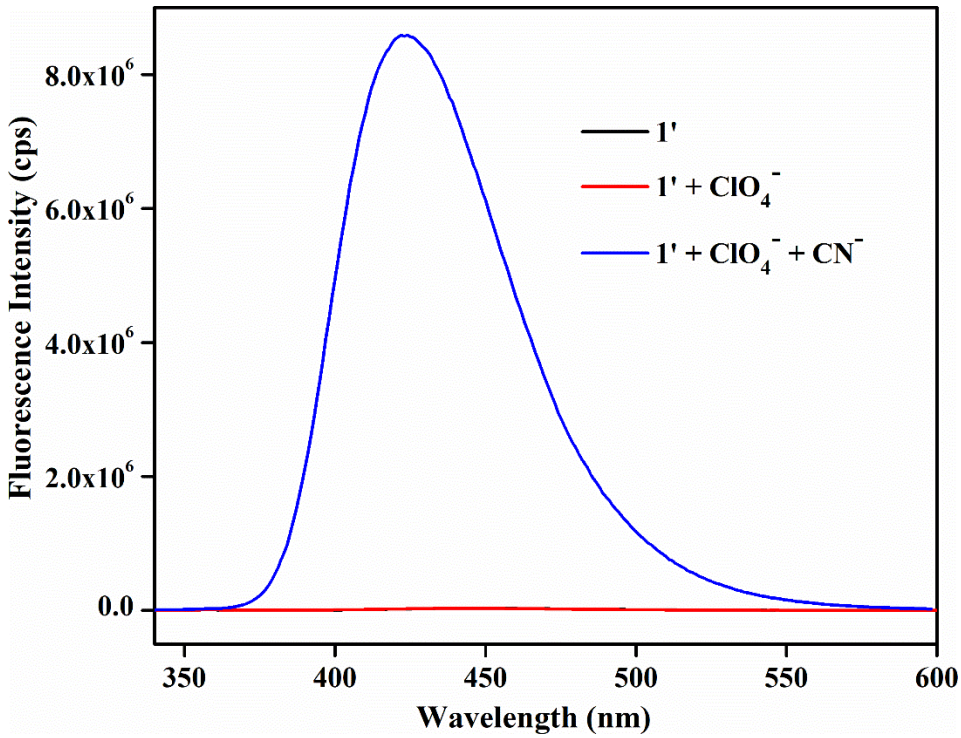

Figure S16. Fluorescence intensity of **1'** dispersed in water after addition of 10 mM solution of NaCN in water (300 µL) in presence of 10 mM solution of $NaClO_4$ in water (300 µL).

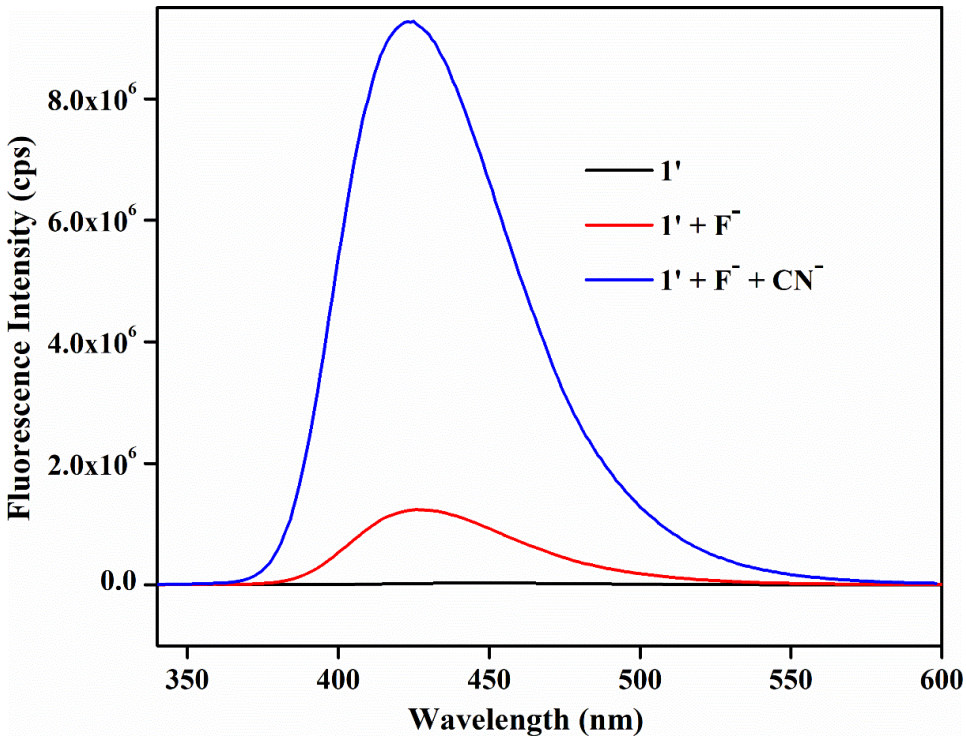

Figure S17. Fluorescence intensity of **1′** dispersed in water after addition of 10 mM solution of NaCN in water (300 µL) in presence of 10 mM solution of NaF in water (300 µL).

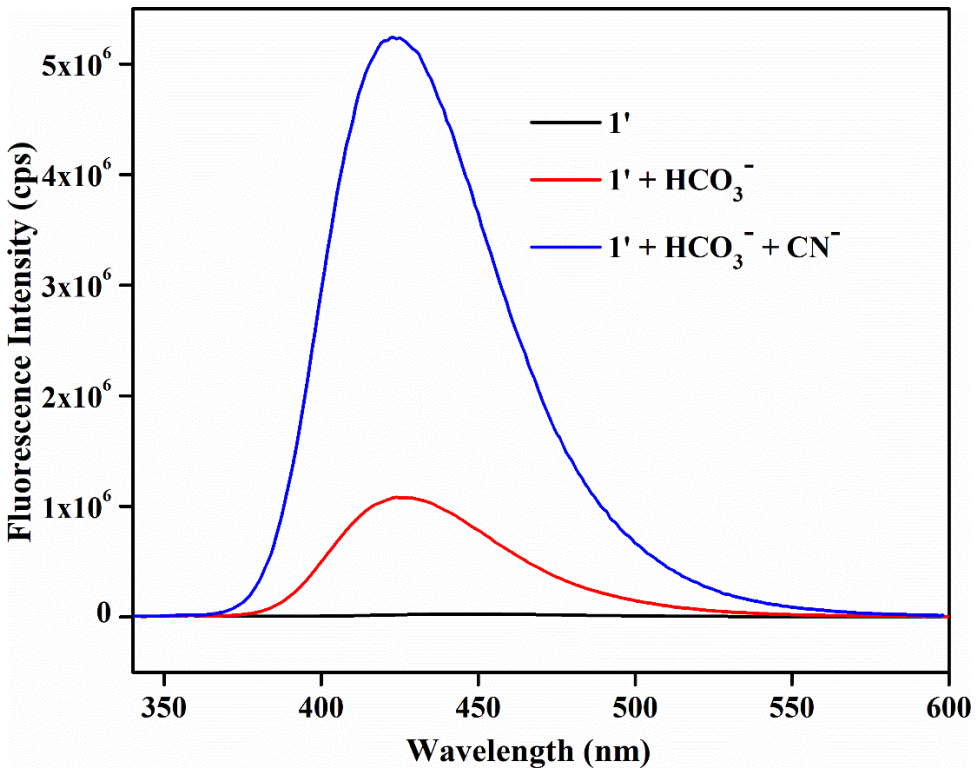

Figure S18. Fluorescence intensity of **1′** dispersed in water after addition of 10 mM solution of NaCN in water (300 µL) in presence of 10 mM solution of $NaHCO_3$ in water (300 µL).

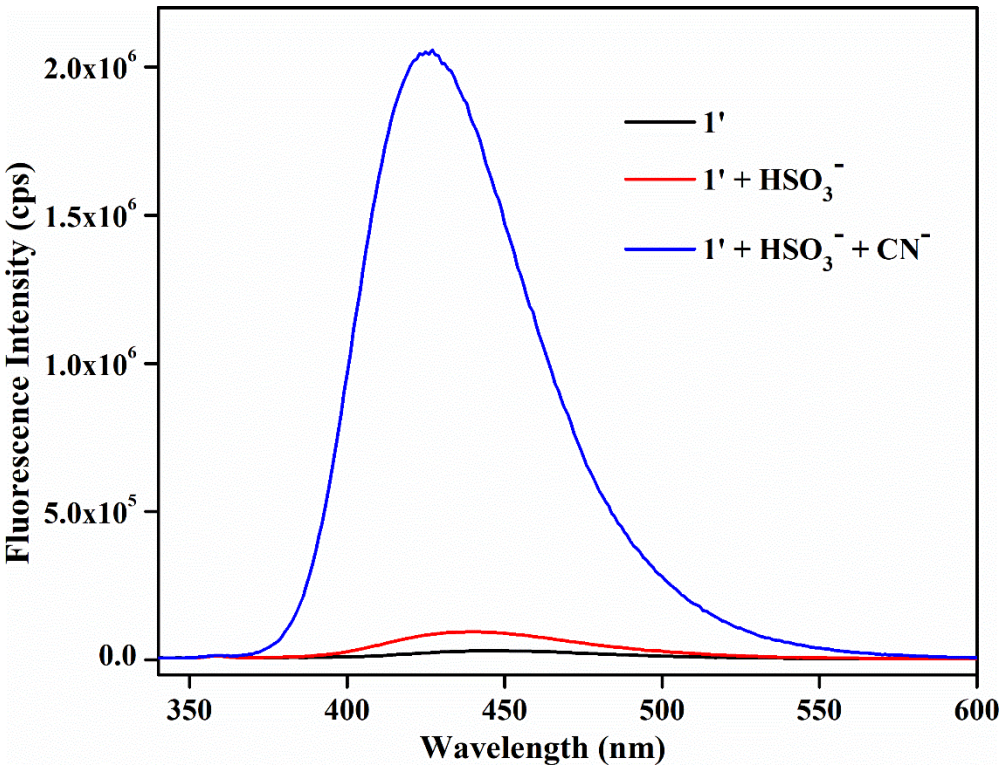

Figure S19. Fluorescence intensity of **1′** dispersed in water after addition of 10 mM solution of NaCN in water (300 µL) in presence of 10 mM solution of $NaHSO_3$ in water (300 µL).

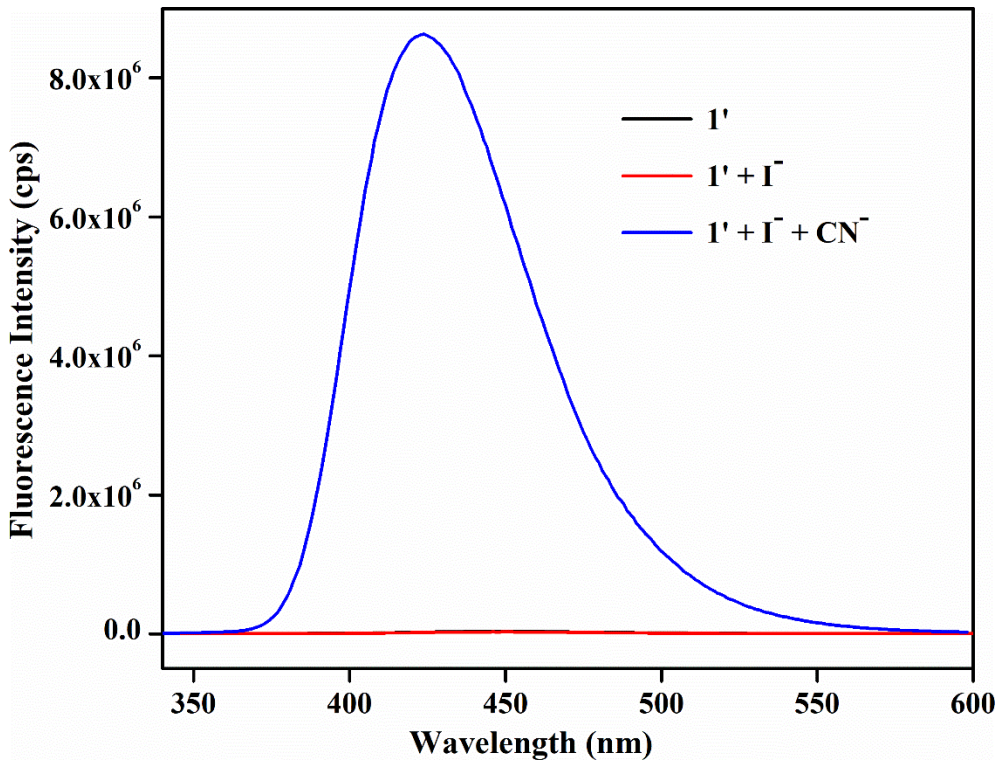

Figure S20. Fluorescence intensity of **1'** dispersed in water after addition of 10 mM solution of NaCN in water (300 µL) in presence of 10 mM solution of NaI in water (300 µL).

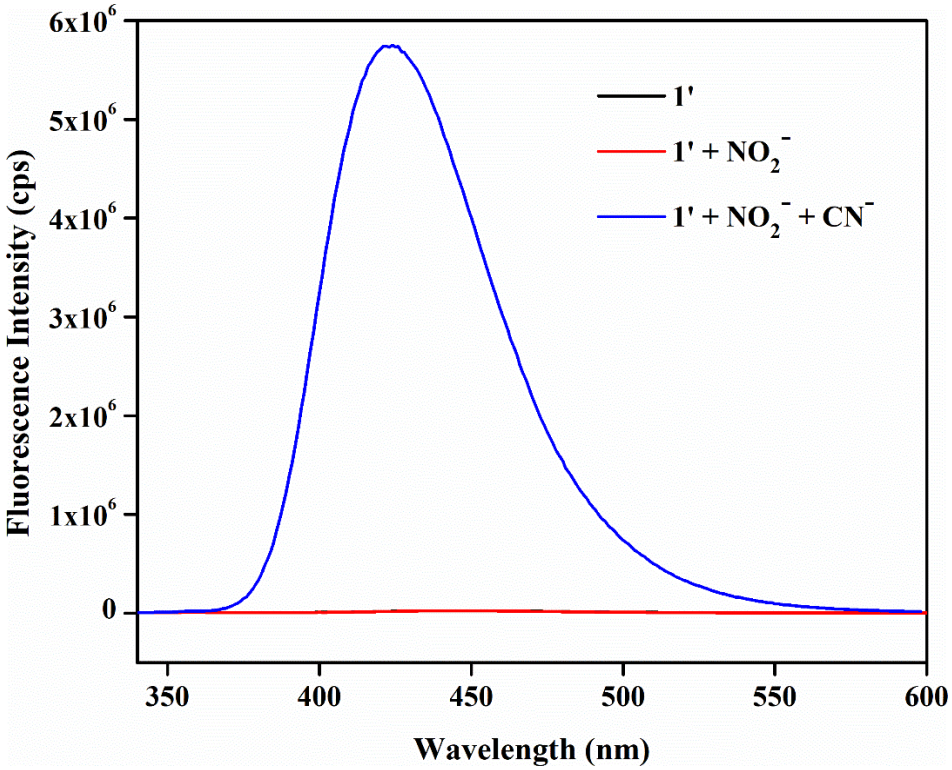

Figure S21. Fluorescence intensity of **1′** dispersed in water after addition of 10 mM solution of NaCN in water (300 µL) in presence of 10 mM solution of $NaNO_2$ in water (300 µL).

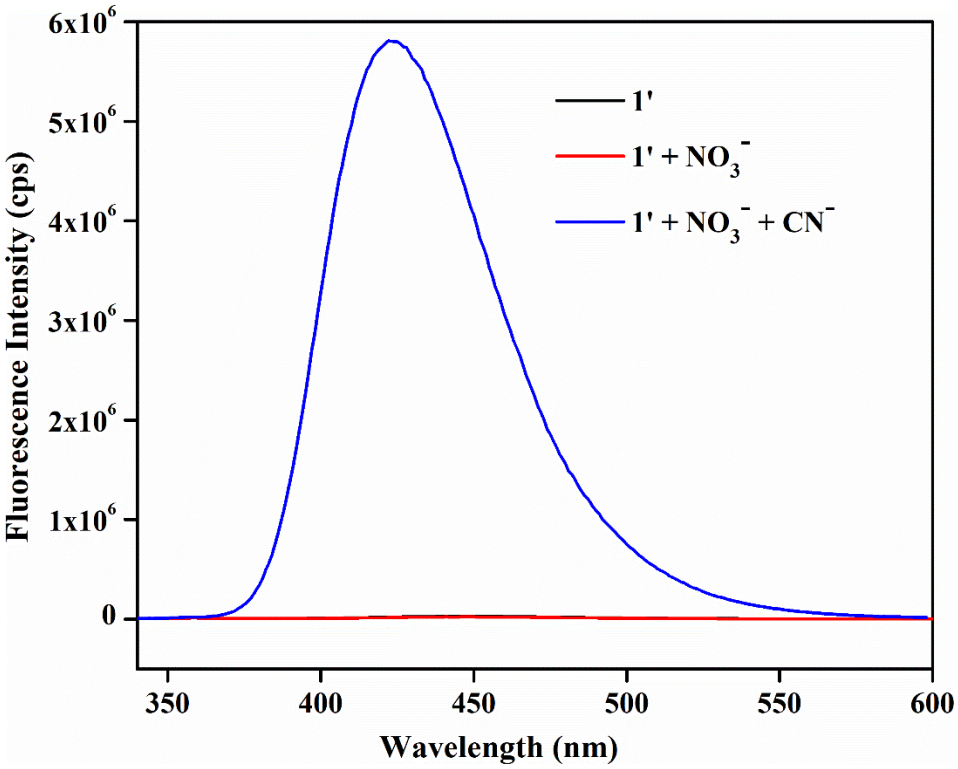

Figure S22. Fluorescence intensity of **1′** dispersed in water after addition of 10 mM solution of NaCN in water (300 µL) in presence of 10 mM solution of $NaNO_3$ in water (300 µL).

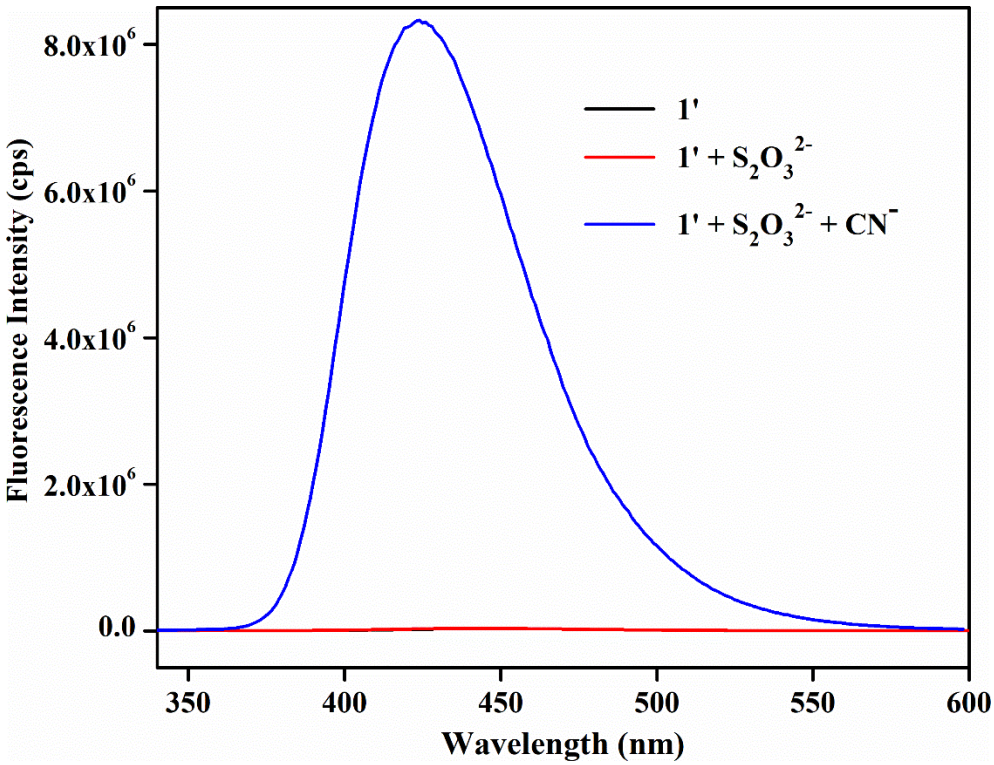

Figure S23. Fluorescence intensity of **1′** dispersed in water after addition of 10 mM solution of NaCN in water (300 µL) in presence of 10 mM solution of $Na_2S_2O_3$ in water (300 µL).

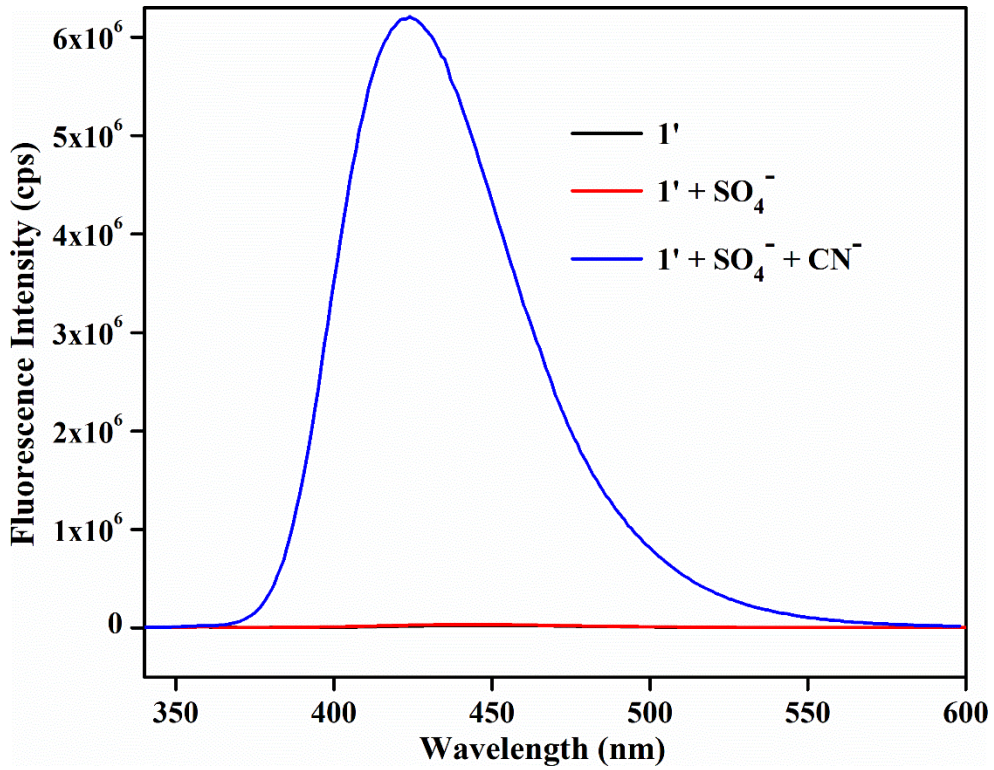

Figure S24. Fluorescence intensity of **1′** dispersed in water after addition of 10 mM solution of NaCN in water (300 µL) in presence of 10 mM solution of Na_2SO_4 in water (300 µL).

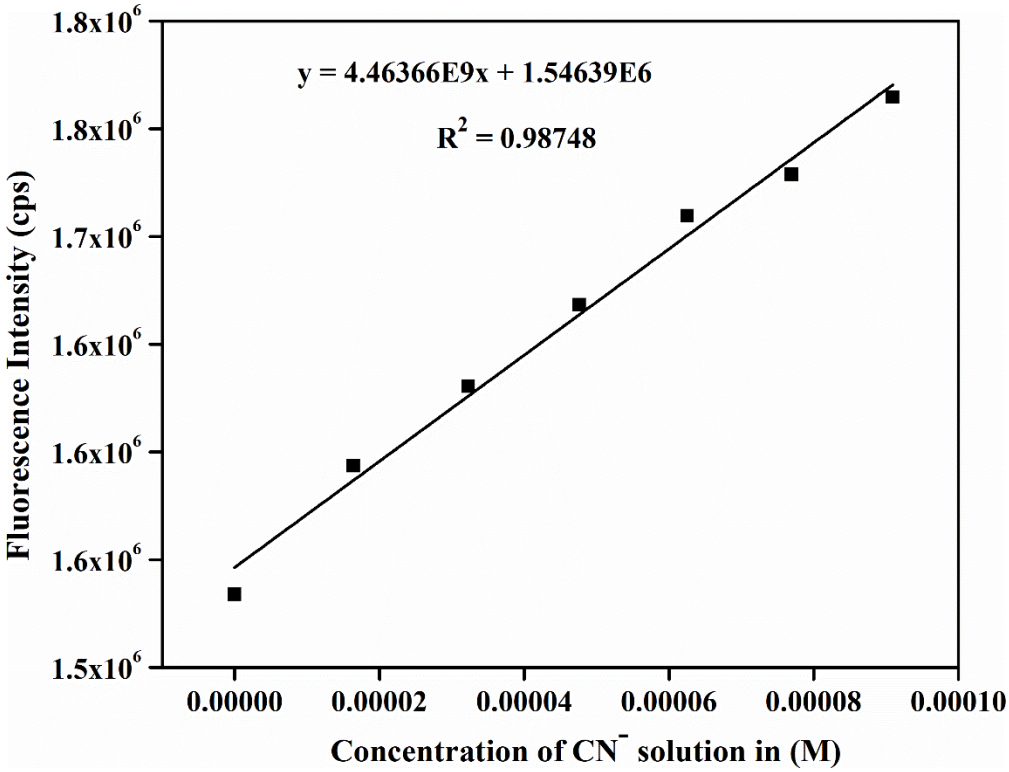

Figure S25. Change in the fluorescence intensity of **1′** as a function of CN^- concentration.

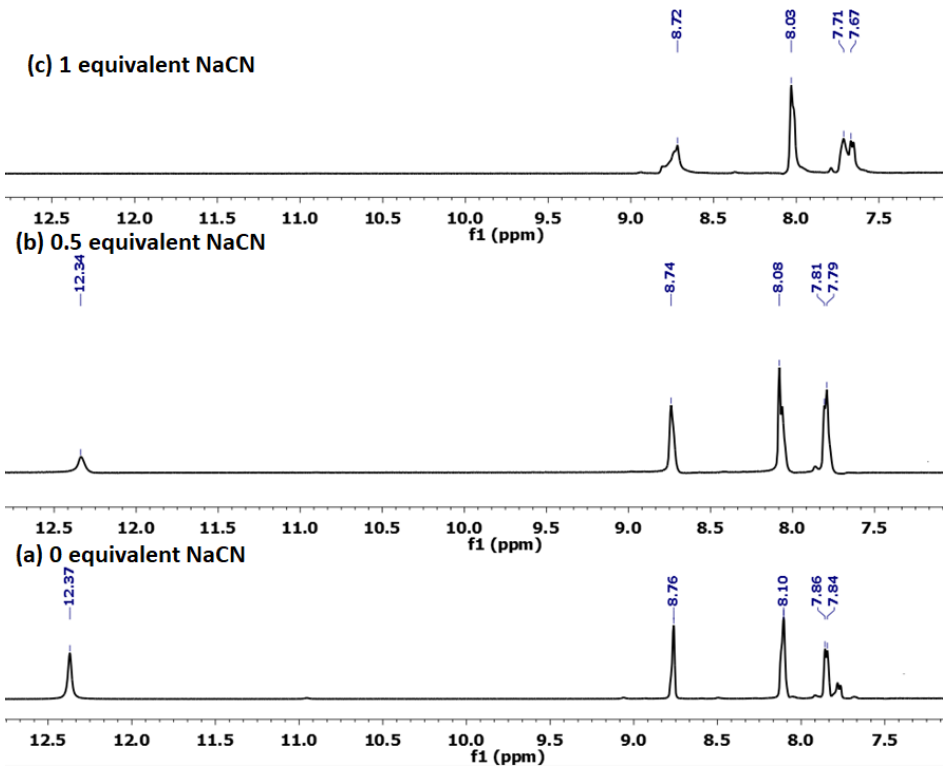

Figure S26. Extended view of stacked ^{1}H NMR spectra of NaCN-treated **1′** after digestion in DMSO-d_6/HF. (a) **1'** (digested in DMSO-d_6/HF), (b) 0.5 equivalent NaCN-treated (dissolved

in D_2O) **1′** (digested in DMSO-d_6/HF), (C) 1 equivalent NaCN-treated (dissolved in D_2O) **1′** (digested in DMSO-d_6/HF). With incremental treatment of NaCN the intensity of peak at 12.37 ppm for –NH proton decreased and shifted to up-field. The other peaks at aromatic region also shifted to up-field region which supports the deprotonation mechanism of –NH group.

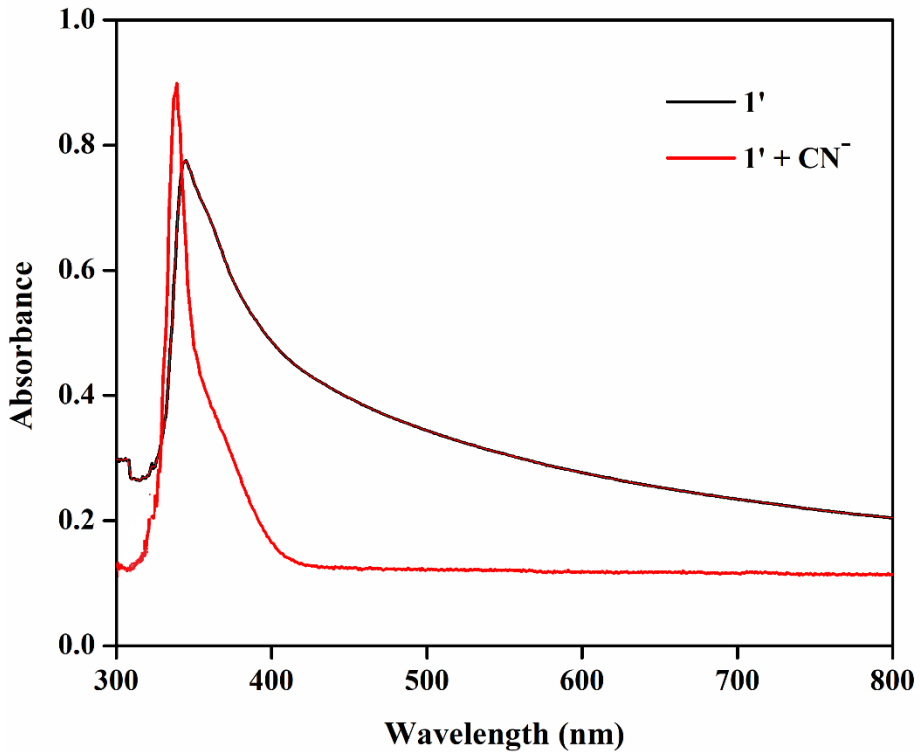

Figure S27. UV-Vis spectra of **1′** before and after addition of CN^- solution (300 µL, 10 mM).

Table S2. Comparison of the solvent, response time, detection limit and fold increament of various existing MOF probes for the fluorescence detection of CN^-.

Sl. No.	Name of MOF	Medium Used	Response Time	Detection Limit	Fold Increment	Ref.
1	DUT-52-NH-$COCF_3$	water	2 min	0.23 µM	3	5
2	CAU-10-N_2H_3	water	2 min	0.48 µM	-	6
3	carbazole-functionalized UiO-67	water	-	0.14 µM	-	7

4	M-ZIF-90	DMSO/Water	-	2 μM	-	8
5	Bio-MOF-1 ⊃ DAAC	HEPES buffer	-	5.2 ppb	17	9
6	Tb-ADP-Bipy	water	10 sec	30 nM	20	10
7	NU-1000-BzTz	Water	-	1.08 μM	-	11
8	hemicyanine-functionalized mixed-ligand PCN-700	water	1 min	0.05 μM	-	12
9	P-**1′**	THF/Water	5 min	0.35 μM	14	13
10	TIP-Co	THF-water	40 min	89.3 nM	-	14
11	UiO-66-NH-$COCF_3$ **(1′)**	Water	1 min	0.28 μM	300	this work

Measurement of quantum yield:

The quantum is defined as the ratio of photon emmited and the ratio of photon absorbed. Here, we have calculated the quantum yield of cyanide treated **1′** by Parker-Rees method[15] using quinine sulphate as reference (0.5 M H_2SO_4). The formula for quantum yield calculation by Parker-Rees method is as follows.

$$\Phi_s = (A_r F_S n_s^2 / A_s n_r F_r^2) \Phi_r \qquad (1)$$

where Φ_r is the quantum yeild of reference 0.5 M quinine sulphate solution and Φ_r is the quantum yield of sample. A_r and A_s are the absorbance of reference and samples respectively. F_r and F_s are the intigrated area of fluroscence intensity for reference and samples respectively and n_r and n_s are the refractive indices of refence and samples respectively. The quantum yield and the photophysical parameters are given below in Table S3.

Table S3. Photophysical parameters for UiO-66-NH-$COCF_3$ after treatment with cyanide solution for the calculation of quantum yield.

Sl. No.	Sample Name	Excitation Wavelength λ_{ex} (nm)	Absorbance (A)	Area of Integrated Fluorescence Intensity (F)	Quantum Yield (ϕ)
1	Quinine Sulphate	310	0.068	8.02 E +08	0.054
2	UiO-66-NH-$COCF_3$**(1′)**	320	0.105	5.41 E +06	0.002
3	**1′**-after inclusion with cyanide solution.	320	0.072	1 E +08	0.063

References:

1. Dalapati, R.; Nandi, S.; Gogoi, C.; Shome, A.; Biswas, S., Metal–organic framework (MOF) derived recyclable, superhydrophobic composite of cotton fabrics for the facile removal of oil spills. *ACS Appl. Mater. Interfaces* **2021,** *13*, 8563–8573.
2. Boultif, A.; Louër, D., Indexing of powder diffraction patterns for low-symmetry lattices by the successive dichotomy method. *J.Appl. Crystallogr* **1991,** *24*, 987-993.
3. *STOE WinXPOW* version 2.11; Stoe & Cie GmbH: Darmstadt, Germany. **2005**.
4. Jakobsen, S.; Gianolio, D.; Wragg, D. S.; Nilsen, M. H.; Emerich, H.; Bordiga, S.; Lamberti, C.; Olsbye, U.; Tilset, M.; Lillerud, K. P., Structural determination of a highly stable metal-organic framework with possible application to interim radioactive waste scavenging: Hf-UiO-66. *Phys. Rev. B* **2012,** *86*, 125429.
5. Gogoi, C.; Nagarjun, N.; Roy, S.; SK, M.; Volkmer, D.; Dhakshinamoorthy, A.; Biswas, S., A Zr-based metal–organic framework with a DUT-52 structure containing a trifluoroacetamido-functionalized linker for aqueous phase fluorescence sensing of the cyanide ion and aerobic oxidation of cyclohexane. *Inorg. Chem.* **2021,** *60*, 4539–4550.
6. Dalapati, R.; Nandi, S.; Reinsch, H.; Bhunia, B. K.; Mandal, B. B.; Stock, N.; Biswas, S., Fluorogenic naked-eye sensing and live-cell imaging of cyanide by a hydrazine-functionalized CAU-10 metal–organic framework. *CrystEngComm* **2018,** *20*, 4194-4201.
7. Das, A.; Biswas, S., A multi-responsive carbazole-functionalized Zr(IV)-based metal-organic framework for selective sensing of Fe(III), cyanide and p-nitrophenol. *Sens. Actuators B Chem.* **2017,** *250*, 121-131.
8. Karmakar, A.; Kumar, N.; Samanta, P.; Desai, A. V.; Ghosh, S. K., A post-synthetically modified MOF for selective and sensitive aqueous-phase detection of highly toxic cyanide ions. *Chem.--Eur. J.* **2015,** *22*, 864-868.
9. Karmakar, A.; Joarder, B.; Mallick, A.; Samanta, P.; Desai, A. V.; Basua, S.; Ghosh, S. K., Aqueous phase sensing of cyanide ions using a hydrolytically stable metal–organic framework. *Chem. Commun.* **2017,** *53*, 1253-1256.
10. Wang, L.; Wang, S.; Chen, Y., Detection of cyanide via extended π-conjugation-induced fluorescence enhancement of a metal organic framework composed of terbium(III), bipyridyl and adenosine diphosphate. *Microchimica Acta* **2017,** *184*, 4597-4602.

11. L, L.; Mercuri, G.; Islamoglu, T.; Fermi, A.; Bergamini, G.; Giambastiani, G.; Rossin, A., Benzothiazolium-functionalized NU-1000: a versatile material for carbon dioxide adsorption and cyanide luminescence sensing. *J. Mater. Chem. C* **2020,** *8*.
12. Li, J.; Yuan, S.; Qin, J.-S.; Pang, J.; Zhang, P.; Zhang, Y.; Huang, Y.; Drake, H. F.; Liu, W. R.; Zhou, H.-C., Stepwise assembly of turn-on fluorescence sensors in multicomponent metal–organic frameworks for in vitro cyanide detection. *Angew. Chem. Int. Ed.* **2020,** *59*, 9319-9323.
13. Dalapati, R.; Nandi, S.; Biswas, S., Post-synthetic modification of a metal–organic framework with a chemodosimeter for the rapid detection of lethal cyanide via dual emission. *Dalton Trans.* **2020,** *49*, 8684-8692.
14. Liu, Y.; Qiu, Q.; Zhang, X.; Huang, K.; Qin, D., Tetra-imidazole functionalized pyrene for constructing Co-MOF and Its application for sensing of cyanide ion. *J. Solid State Chem.* **2021,** *300*, 1222582.
15. Parker, C. A.; Rees, W. T., Correction of fluorescence spectra and measurement of fluorescence quantum efficiency. *Analyst* **1960,** *80*, 587-600.